Role of surface-bound hole states in electric-field-driven superconductivity at the (110)-surface of diamond

Kazuhiro Sano,* Takahiro Hattori, and Kohji Nakamura
Department of Physics Engineering, Mie University, Tsu, Mie 514-8507, Japan
(Received 9 January 2017; revised manuscript received 16 September 2017; published 30 October 2017)

Hole states in electric-field-driven superconductivity at the (110)-surface of diamond are examined by means of first-principles calculations and one-dimensional tight-binding model calculations. It is found that surface-bound hole states confined near the surface by application of an electric field E play a key role in superconductivity. Indeed, there is a critical external electric field $|E_c|$ ($\simeq$0.4 V/Å) for observing the superconductivity, which can be attributed to the second surface-bound hole state. With McMillan's formula and calculated phonon-electron coupling constants, we demonstrate that, in electric fields $<|E_c|$ which correspond to a surface carrier density of $\sim 2.3 \times 10^{13}$ cm^{-2}, superconductivity may not be practically observed while the superconductivity transition temperature suddenly increases at $|E_c|$.

DOI: 10.1103/PhysRevB.96.155144

I. INTRODUCTION

Recent progress in electric-double-layer (EDL) fabrication methods using ionic liquids opens a new vista for electric-field-driven superconductivity [1–4]. Carriers induced at surfaces by application of an electric field (E) may be uniformly confined to a sheetlike region within a depth of $\sim 10^{-7}$ cm from the surface [5,6]. Experimentally, the induced carrier density reaches up to 10^{14} cm^{-2} in $SrTiO_3$ and MoS_2 [2], and superconductivity has been successfully observed, the transition temperatures, T_c's, are comparable to those in the bulk with chemical dopings [2,7,8]. Although the induced carriers are limited to surfaces, they are free from the influence of unavoidable randomness by chemical dopings so that they can be treated as ideally pure and clean systems. Moreover, T_c is generally believed to be high at a clean limit [9,10] and the intrinsic ability of superconductors may be brought out by means of the electric-double-layer method.

In diamond, owing to the large phonon frequency of 150 meV, much interest in superconductivity has been raised [10–15]. Experiments [12,13] showed that boron dopants in diamond induce superconductivity at 7–9 K with a carrier density of 10^{22} cm^{-3}. First-principles calculations within the virtual crystal approximation [14,15] further revealed that superconductivity is dominated by optical phonon modes near the Brillouin zone (BZ) center. Although T_c tends to increase as the boron concentration increases, unavoidable structural disorders and impurity bands may cause suppression of T_c in a heavy doping region [12].

Alternately, electric-field-driven superconductivity at the (110)-surface of hydrogenated diamond was proposed from first-principles calculations [16–18]. The hole carrier density, confined within a few carbon layers (of thickness $\sim$10 Å) from the surface, exceeds the critical value of the carrier density of the boron-doped diamond. Because the calculated electron-phonon coupling constants are comparable in magnitude to that in the boron-doped diamond, the results suggest the possibility of electric-field-driven superconductivity.

In parallel, experiments on electric-field-driven superconductivity were conducted for the (111)-surface and (100)-surface of diamond [3,4], and precursory phenomena of superconductivity were observed [19,20], where the temperature dependence of surface resistivity is almost constant at low temperature. The typical achieved induced charge density at surfaces is $\sim 4 \times 10^{13}$ cm^{-2}, which corresponds to $|E| \simeq 0.7$ V/Å [21]. However, superconductivity has not been observed experimentally. Although reconstructions at the (111)-surface and (100)-surface of diamond may be unavoidable [22–24], it is worthwhile to revisit theoretically the electric-field-driven superconductivity in the (110)-surface of diamond.

In the present work, we investigate the role of surface hole states (surface-bound hole states) induced by application of an electric field. We importantly find that there is a critical external electric field, E_c, for observing superconductivity, which can be attributed to the second surface-bound hole state. Calculations based on a one-dimensional tight-binding model have further proven the nature of the surface-bound hole states in sufficiently thick systems. With McMillan's formula and calculated phonon-electron coupling constants, the estimated T_c as a function of $|E|$ shows that, in electric fields $<E_c$, superconductivity may not be practically observed while T_c suddenly increases at $|E_c|$.

II. MODEL AND METHOD

An EDL system of the (110)-surface of diamond is modeled by a single slab, consisting of carbon layers with hydrogen terminations at both sides of the slab, as shown in Fig. 1(a). The dashed-line frame in the figure represents a unit cell of a 13-carbon-layer model (C26H4), which contains 26 carbon atoms and 4 hydrogen atoms. Calculations were performed based on density functional theory by using Quantum ESPRESSO (QE) software [25], where atomic positions are used for the values calculated previously [16,17]. The hydrogen termination, as demonstrated previously [16–18], removes dangling bonds that appear on the clean surface and stabilizes the surface structure. It is noted that the effect of hydrogen termination may be small in surface electronic states, because the hole

*sano@phen.mie-u.ac.jp

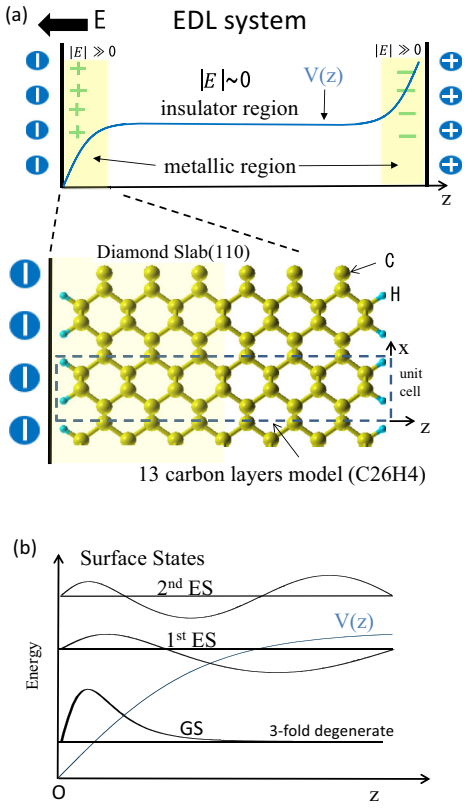

FIG. 1. (a) Schematic diagram of an EDL system of a diamond slab with an electric potential $V(z)$ and a 13-carbon-layer model (C26H4) for the (110)-surface of hydrogenated diamond in a negative electric field, where the dashed line frame represents a unit cell on the x–z plane. (b) Schematic diagrams of wave functions of surface-bound hole states (thick solid lines) and the corresponding hole eigenstates (horizontal thin lines). $V(z)$ stands for a screened potential of holes as a function of the position z.

density is very small at the position of the hydrogen atoms [16–18]. The top of the valence band in hydrogenated diamond consists of electron orbitals in carbons below the hydrogen layer, and the contribution of the hydrogens to the top of the valence band is negligibly small.

Because an external electric field concentrates holes near the surface, surface-bound hole states may be discreetly formed, as shown in Fig. 1(b), where the wave function of a ground state (GS) and that of the first excited state (1st ES) and second excited state (2nd ES) are illustrated. In the GS, the holes are confined close to the surface while those in the excited states gradually penetrate into the inside of the system. In the case of the (110)-surface of diamond, the surface-bound state at the Γ point may be lifted into three states (A, B, and C), which correspond to the threefold degenerate states in the bulk [15].

III. RESULTS

A. Band structure in the electric field

The calculated band structure of C26H4 in a negative electric field of $E = -1.0$ V/Å is shown in Figs. 2(a) and 2(b). The figures show that eigenstates of GS^A and GS^B at the Γ point are located above the Fermi level ε_F while the other states are below ε_F. We identify these states by using the hole density distributions as a function of the position, z, as shown in Fig. 2(c). The hole density distributions of GS^A, 1st ES^A, and 2nd ES^A are classified by the number of nodes: zero, one, and two, respectively. The density distributions projected onto the x–z plane of the slab [Fig. 2(d)] further indicate that almost all the holes are concentrated in bonds between the neighboring carbon atoms. For example, the holes in GS^A significantly accumulate in bonds along the x direction near the surface, but for GS^B these are distributed in a zigzag pattern along the z direction.

To examine the dependence of slab thickness, L, on the surface-bound hole states, where L is the number of atomic layers along the z axis in the slabs, we further performed first-principles calculations for C46H4 ($L = 23$), C22H4 (11), and C18H4 (9) models in electric fields of -0.3, -0.5, and -1.0 V/Å. The results are shown in Fig. 3. In all the electric fields, eigenstates at the Γ point behave inversely to L^2. The energy of GS^A decreases when L increases, and it is located above ε_F in the limit of $L = \infty$. For GS^B, the energy changes from negative to positive values when L is larger than 23 layers in -0.5 V/Å (C46H4) and 13 layers in -1.0 V/Å (C26H4). However, in a weak electric field, e.g., -0.3 V/Å, the energy of GS^B never exceeds ε_F even when $L \to \infty$. Thus there is a critical electric field at which the GS^B band crosses ε_F. In contrast, the remaining bands with lower energy than that in GS^B are always below ε_F, indicating that these states never contribute to the hole carriers. By using the results of electric fields of -0.3, -0.4, and -0.5 V/Å, the critical electric field E_c in the limit of $L = \infty$ is estimated to be ~ -0.4 V/Å.

B. Tight-binding model analysis

To confirm the surface-bound hole states in the limit of $L = \infty$, we performed calculations based on the one-dimensional tight-binding model, employing systems with system size of L^{TB} up to 300 atomic sites, where the charge screening effect to an electric field is incorporated by solving a discretized Poisson's equation self-consistently [5,6]. The Hamiltonian for the one-dimensional tight-binding model may be given by

$$H = -t \sum_i (c_i^\dagger c_{i+1} + \text{H.c.}) + V(z_i) n_i, \qquad (1)$$

where $n_i = c_i^\dagger c_i$ and $c_i^\dagger$ (c_i) is a creation (annihilation) operator of an electron at site i. $V(z_i)$ is the electric potential at atomic position z_i, which is determined by the discretized Poisson's equation as

$$\frac{V(z_{i+1}) - 2V(z_i) + V(z_{i-1})}{a^2} = -q\langle n_i \rangle / (\epsilon_r \epsilon_0), \qquad (2)$$

where a is a distance between the nearest-neighboring atomic sites (1.26 Å) and q is a charge that corresponds to the hole density in the system. $\langle n_i \rangle$ is an expectation value of n_i, and ϵ_0 and ϵ_r are the vacuum and relative permittivities, respectively. ϵ_r is assumed to be the bulk value of 5.68. The transfer energy, t, is fitted in such a way that eigenstates in the ground state (GS^{TB}) and first excited state (1st ES^{TB}) of the holes in a model of $L^{TB} = 13$ match those in GS^A and the 1st ES^A of C26H4 ($L = 13$) in the first-principles calculations. The

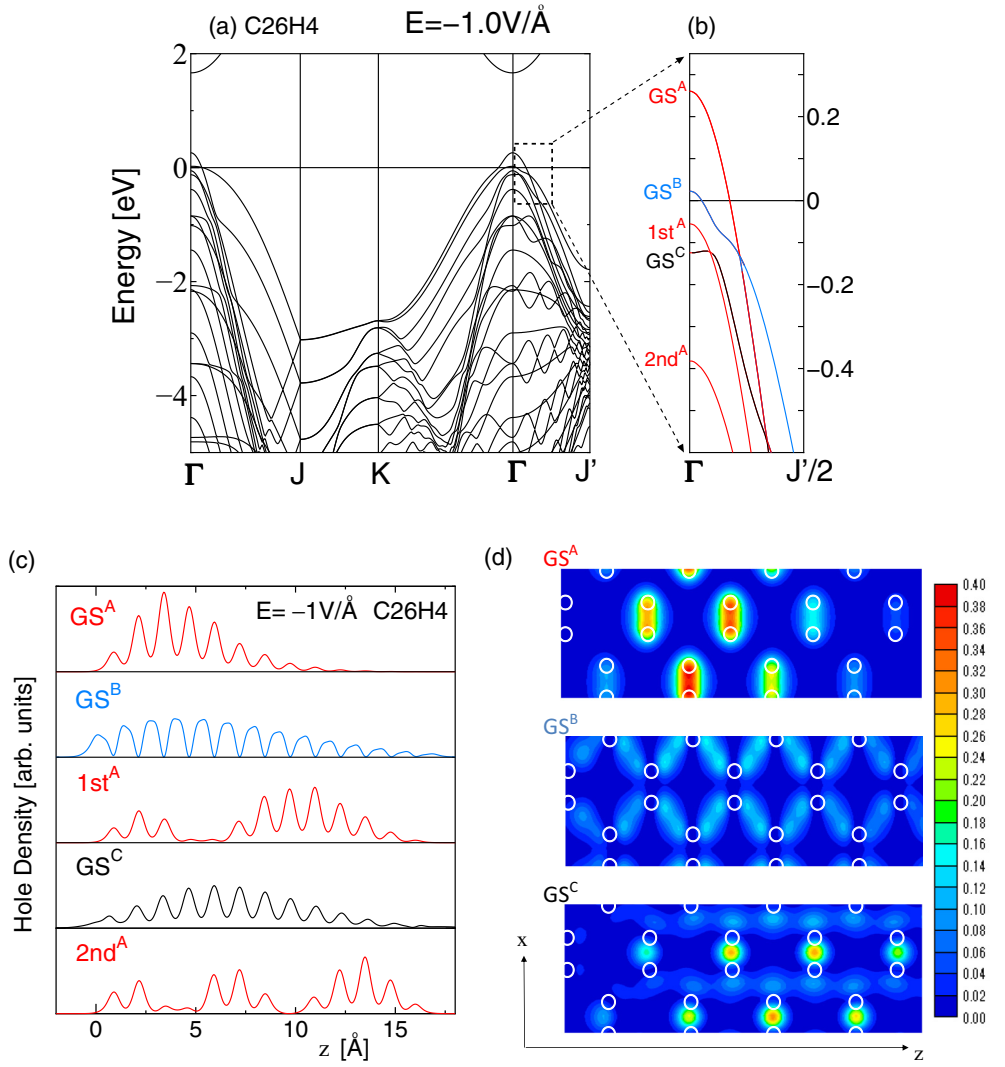

FIG. 2. (a) Calculated band structure of C26H4 for $E = -1.0$ V/Å, where the Fermi energy, ε_F, is set to zero. The holes emerge at around the Γ point. (b) An enlarged figure of the band structure near ε_F in (a), where the hole bands are classified by the character of the hole density distribution. (c) The induced hole density distributions from the surface to the inside of the crystal, which correspond to the hole states in (b). (d) The projected hole density distributions on the x–z plane, where white empty circles represent carbon atoms.

transfer energy t results in 1.92 in an electric field of -1 V/Å, which corresponds to an effective mass (m^*) of 2.5 [26]. The calculated hole density distributions in the tight-binding model agree with those in the first-principles calculations, as shown in the inset of Fig. 4(a).

The wave functions of GS^{TB}, 1st ES^{TB}, and 2nd ES^{TB} as a function of z_i in a model of $L^{TB} = 300$ in -1 V/Å [Fig. 4(a)] clearly demonstrate that not only GS^{TB} but also the 1st ES^{TB} behave as bound states near the surface. In contrast, the wave function of the 2nd ES^{TB} largely spreads into the inside of the system. The value of $V(z_i)$ is almost constant except near the surface. This suggests that the charge screening effect efficiently reduces the electric field in ∼10 layers from the surface and the induced holes may be confined to the surface, as pointed out previously [16].

Figure 4(b) shows an extrapolation of the energies with respect to L^{TB} in -1 V/Å. This indicates that GS^{TB} is located above ε_F and that the other states except for the 1st ES^{TB} are below ε_F in the limit of $L^{TB} = \infty$. The results indicate that the eigenstates above ε_F represent surface-bound states; those orbitals are localized and are confined near the surface, as seen in Fig. 1(b). The remaining states being below ε_F are unbound states; those orbitals spread out inside the crystal. As shown in the inset, the 1st ES^{TB} at $L^{TB} = \infty$ is above ε_F, which forms a surface-bound state, although the energy gap between the 1st ES^{TB} and ε_F is very small. When the magnitude of the electric field decreases, however, the energy of the 1st ES^{TB} goes below ε_F, being an unbound state, and the orbital spreads out inside the crystal, as illustrated in Fig. 4(c). This reflects the critical electric field of the surface-bound state, as demonstrated in GB^B in the previous subsection. The hole distribution of GB^{TB}, $|\Phi(z_i)|^2$, has almost no size dependence on L^{TB}, as shown in Fig. 4(d) for both -0.3 and -1.0 V/Å, where $|\Phi(z_i)|^2$ as a function of the atomic position is plotted for models of $L^{TB} = 13$ and $L^{TB} = 300$. The confined length of the induced holes near the surface for both systems is ∼10 Å.

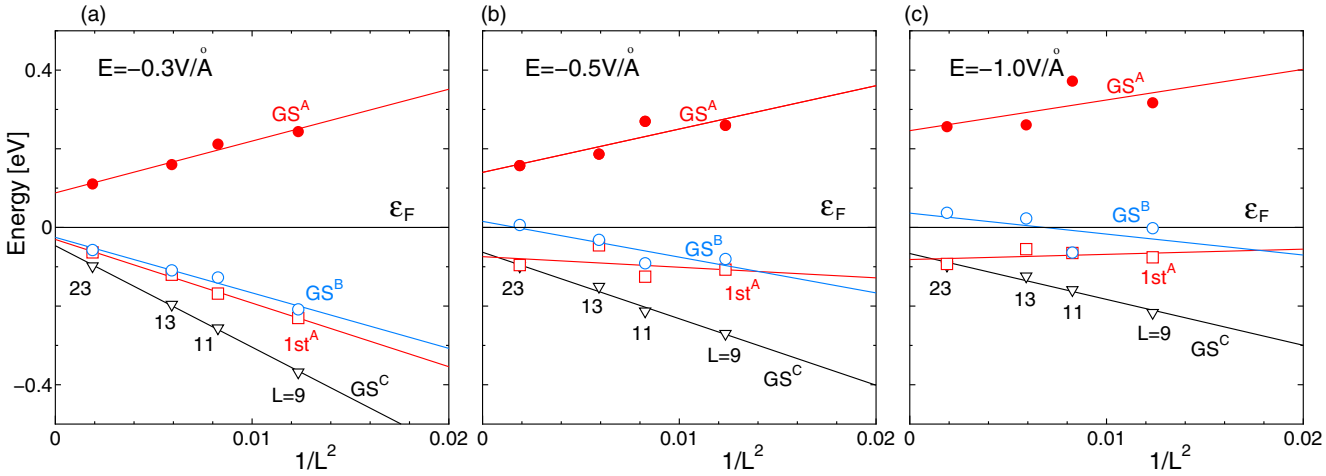

FIG. 3. Energy levels of hole bands at the Γ point with respect to slab thickness, L (in units of the number of layers), in electric fields E of (a) -0.3, (b) -0.5, and (c) -1.0 V/Å, where $L = 23$ corresponds to C46H4. Solid circles represent energies of the topmost bands in the valence states (GS^A), and open circles, squares, and triangles are those of the second (GS^B), third (1st ES^A), and fourth (GS^C) bands from the top bands, respectively.

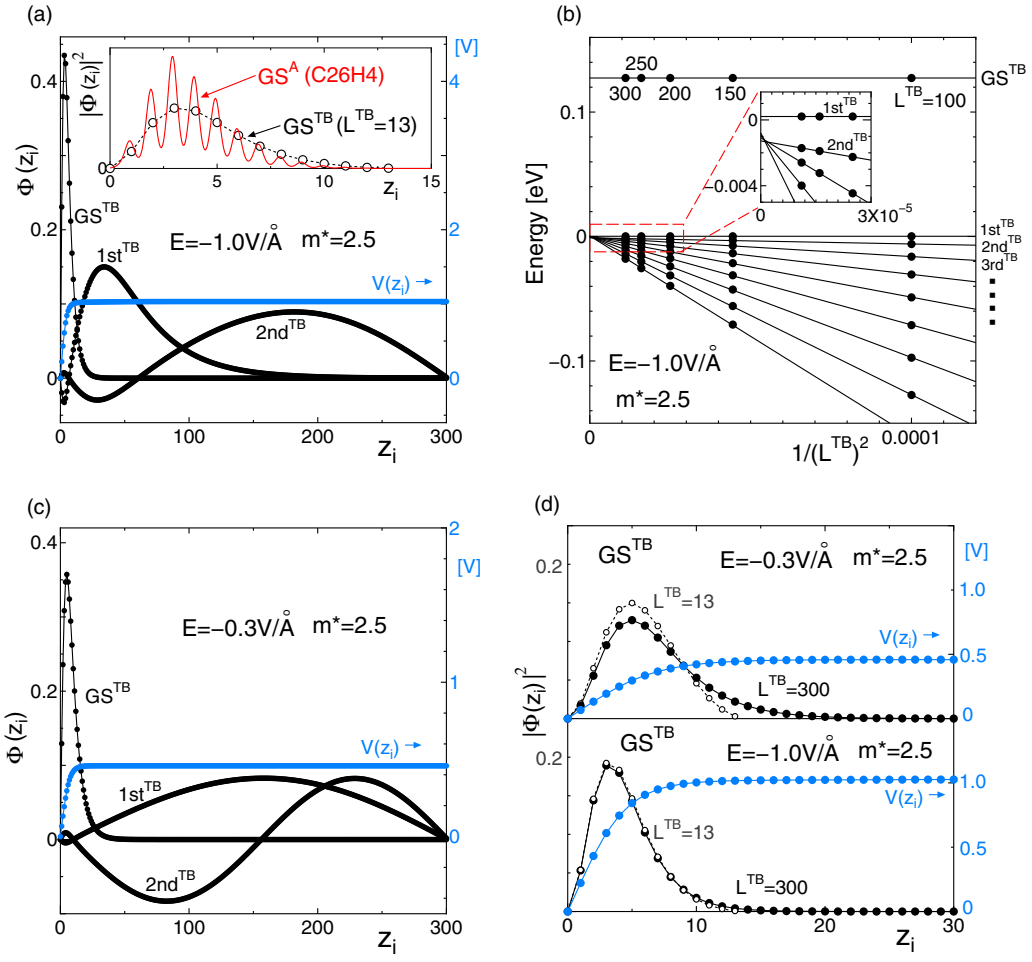

FIG. 4. (a) Calculated wave functions $[\Phi(z_i)]$ in the tight-binding model for a system with thickness of $L^{TB} = 300$ (in units of the number of atoms) in $E = -1.0$ V/Å. The inset shows the hole density distribution $|\Phi(z_i)|^2$ for $L^{TB} = 13$ (empty circles with a dotted line) and that of GS^A in C26H4 ($L = 13$) obtained by first-principles calculations (solid line). (b) An extrapolation of the energy levels in the tight-binding model with respect to L in $E = -1.0$ V/Å. The inset shows an enlarged region near ε_F. (c) The wave functions in the tight-binding model for a system with $L^{TB} = 300$ in $E = -0.3$ V/Å. (d) The hole density distribution $|\Phi(z_i)|^2$ in $L^{TB} = 300$ (solid circles with solid lines) and $L^{TB} = 13$ (empty circles with dotted lines) obtained by using the tight-binding model with $E = -0.3$ V/Å (upper panel) and -1.0 V/Å (lower panel).

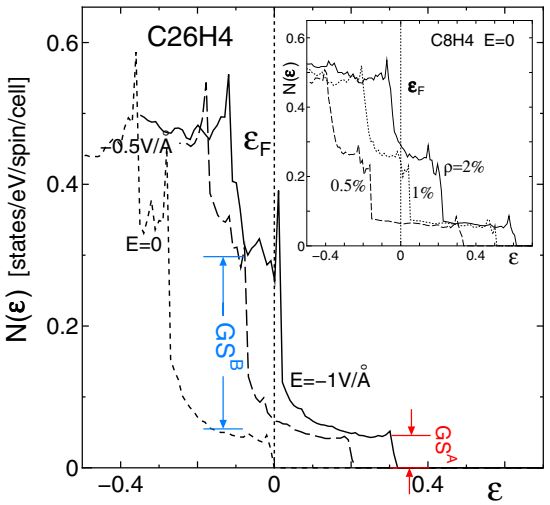

FIG. 5. Calculated DOS, $N(\varepsilon)$, of C26H4 in electric fields (E) of 0, −0.5, and −1 V/Å. The inset shows the DOS of C8H4 with hole concentrations (ρ_h) of 0.5%, 1.0%, and 2.0%. A typical feature of 2D DOS with steps appears around the valence top.

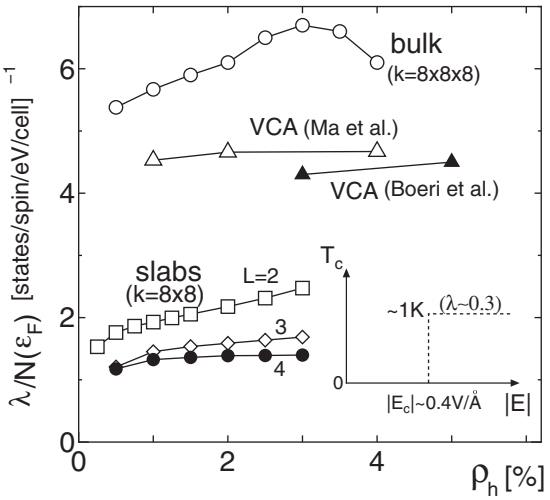

FIG. 6. $V_p[=\lambda/N(\varepsilon_F)]$ of C4H4 ($L=2$), C6H4 (3), and C8H4 (4) obtained by using 8×8 k points as a function of hole concentration. The results of bulk systems and VCA are also shown. The inset shows a schematic diagram of T_c as a function of E.

C. Density of states and transition temperature T_c

To estimate T_c of electric-field-induced superconductivity of the (110)-surface of diamond, we consider the density of states (DOS), $N(\varepsilon)$, as a function of the energy, ε, and the phonon-electron coupling constant, λ. As shown in the previous subsections, the electronic state of diamond slabs is characterized by a few surface states. The two-dimensional (2D) behavior of these states is clearly apparent in $N(\varepsilon)$ as a function of energy, ε. Figure 5 shows the DOS of C26H4 in electric fields of 0, −0.5, and −1 V/Å, calculated by using first-principles calculations, where ε_F is set to zero and 100×100 k points in the 2D BZ are used. The first step in the DOS at the valence top is due to the formation of GS^A, and the second one has additional contributions from GS^B, i.e., GS^A+GS^B. The height of the second step (∼0.27 states/eV/spin/unit cell) is rather larger than that of the first one (∼0.07) by a factor of 4, and thus GS^B contributes largely to the DOS. Note that the edge of the second step is close to ε_F when the electric field reaches ∼1 V/Å, giving a threshold for introducing large DOS at ε_F. This indeed corresponds to the critical electric field of C26H4 ($L=13$), although it is 0.4 V/Å for a system with $L=\infty$ as mentioned previously.

The inset of Fig. 5 indicates that the hole density dependence on the DOS in C8H4 resembles the electric field dependence in C26H4, especially around ε_F, where ρ_h is adjusted by a parameter defined by an average hole concentration. In both models, $N(\varepsilon)$ shows a typical feature of a 2D system with steps in the DOS. The DOS of C6H4 and C4H4 has almost the same features as those of C8H4. However, the computations for λ for large systems such as C26H4 may be difficult and, moreover, a dense k-point mesh may be necessary for reproducing a typical 2D feature in the superconducting state quantitatively, as demonstrated in the DOS of Fig. 5. To overcome this difficulty, first, we analyzed the relationship between λ and the DOS at ε_F, namely, $V_p=\lambda/N(\varepsilon_F)$, by employing results of the C4H4, C6H4, and C8H4 models. Here, V_p corresponds to the so-called attraction of Cooper pairs in BCS theory [27], which may be almost a constant with respect to ρ_h, as demonstrated for picene [28].

Figure 6 summarizes the values of V_p for the slabs of C4H4, C6H4, and C8H4 with $\rho_h=0.5\%$, 1.0%, 1.5%, 2.0%, 2.5%, and 3.0% and those of the bulk. For all the slabs, the value of V_p converges when the number of k points increases when going to 5×5, 6×6, and 8×8 [29], where the numerical error may be canceled out between the calculated λ and $N(\varepsilon_F)$. For the bulk, calculations with $16\times16\times16$ k points were made and a similar convergence is obtained. To estimate V_p of C26H4 ($L=13$) as a sufficiently thick slab (denoted by $V_p^{\rm slab}$), we extrapolated the results of $L=2$, 3, and 4 by assuming a $1/L^2$ dependence, and we obtained $\simeq1.1$ for $0.5\%\leqslant\rho_h\leqslant3.0\%$. Since the ρ_h dependence of $V_p^{\rm slab}$ is small, we may neglect the ρ_h dependence of $V_p^{\rm slab}$ for simplicity and treat it as a constant of 1.1. Next, we approximated the DOS as a simple step function with respect to ε, and we used typical values of C26H4, 0.07 for the first step of GS^A and 0.27 for the second step of GS^A+GS^B in Fig. 5. Then, we derived two values for λ, 0.08 and 0.3, for GS^A and GS^A+GS^B, respectively [30].

With the two λ values, we examined the electric-field dependence of T_c, where the McMillan equation [31,32] was used:

$$T_c\simeq\frac{\omega_{\log}}{1.2}\exp\left(-\frac{1.04\,(1+\lambda)}{\lambda-\mu^*(1+0.62\lambda)}\right).$$

Here, $\omega_{\log}$ is the logarithmic average of the phonon frequency and the calculated value of 1200 K for a diamond slab [33] is used. μ^* is the screened Coulomb pseudopotential, which is usually set as ∼0.1 [13–15,31]. Since recent experiments of superconductivity in 2D systems indicate that the difference in T_c values between 2D and 3D systems is small [34], an appropriate value of μ^* for 2D systems is expected to be close to that of 3D systems. We assumed a typical value of μ^*, 0.1 [15,35]. Since $\varepsilon_F\sim0.2$ eV in the present system, which is comparable to $\omega_{\log}$, the adiabatic condition, $\varepsilon_F\gg\omega_{\log}$, which

is ordinarily assumed in the McMillan equation, does not hold. Our estimation of T_c is therefore semiquantitative.

For the system in the limit of $L = \infty$, the relevant surface state is only GS^A and $\lambda \lesssim 0.1$, when $|E| < |E_c|$ ($\simeq$0.4 V/Å). As a consequence, the calculated value of T_c is $\lesssim 10^{-3}$ K, and superconductivity may not be practically observed, as shown in the inset of Fig. 6. For $|E| > |E_c|$, λ may suddenly increase, because the DOS at ε_F suddenly increases at E_c. As shown in the inset of Fig. 6, the calculated value of T_c is $\sim$1 K, and the critical surface charge density σ_c corresponding to $|E_c|$ is $\sim 2.3 \times 10^{13}$ cm^{-2}. The presence of E_c may be very interesting and would invite further experiments [36].

IV. SUMMARY

We investigated electric-field-driven superconductivity in the (110)-surface of diamond by using first-principles and the one-dimensional tight-binding model calculations. By analyzing the band structures of the semi-infinite thick slabs in the electric fields, the bound states above ε_F in energy are found to form near the surface while the other states below ε_F behave continuously as bulk states. Indeed, we find that there is a critical electric field E_c ($\simeq -0.4$ V/Å) for observing superconductivity, which can be attributed to the second surface-bound hole state. With McMillan's formulation and the calculated phonon-electron coupling constants, we roughly estimate T_c as a function of E. Our result indicates that the calculated T_c is $\sim$1 K, when the magnitude of the electric field is $> |E_c|$, which corresponds to a surface carrier density of $\sim 2.3 \times 10^{13}$ cm^{-2}.

ACKNOWLEDGMENTS

This work was supported by JSPS KAKENHI Grant No. 15K05168. Computations were performed at the Research Institute for Information Technology, Kyushu University.

[1] K. Ueno, S. Nakamura, H. Shimotani, A. Ohtomo, N. Kimura, T. Nojima, H. Aoki, Y. Iwasa, and M. Kawasaki, Nat. Mater. **7**, 855 (2008).
[2] K. Ueno, H. Shimotani, H. Yuan, J. Ye, M. Kawasaki, and Y. Iwasa, J. Phys. Soc. Jpn. **83**, 032001 (2014).
[3] T. Yamaguchi, E. Watanabe, H. Osato, D. Tsuya, K. Deguchi, T. Watanabe, H. Takeya, Y. Takano, S. Kurihara, and H. Kawarada, J. Phys. Soc. Jpn. **82**, 074718 (2013).
[4] Y. Takahide, H. Okazaki, K. Deguchi, S. Uji, H. Takeya, Y. Takano, H. Tsuboi, and H. Kawarada, Phys. Rev. B **89**, 235304 (2014).
[5] M. Dankerl, A. Lippert, S. Birner, E. U. Stützel, M. Stutzmann, and J. A. Garrido, Phys. Rev. Lett. **106**, 196103 (2011).
[6] M. T. Edmonds, C. I. Pakes, and L. Ley, Phys. Rev. B **81**, 085314 (2010).
[7] J. F. Schooley, W. R. Hosler, E. Ambler, J. H. Becker, M. L. Cohen, and C. S. Koonce, Phys. Rev. Lett. **14**, 305 (1965).
[8] J. T. Ye, Y. J. Zhang, R. Akashi, M. S. Bahramy, R. Arita, and Y. Iwasa, Science **338**, 1193 (2012).
[9] D. Belitz, Phys. Rev. B **35**, 1651 (1987).
[10] T. Shirakawa, S. Horiuchi, Y. Ohta, and H. Fukuyama, J. Phys. Soc. Jpn. **76**, 014711 (2007).
[11] G. Savini, A. C. Ferrari, and F. Giustino, Phys. Rev. Lett. **105**, 037002 (2010).
[12] A. Kawano, H. Ishiwata, S. Iriyama, R. Okada, T. Yamaguchi, Y. Takano, and H. Kawarada, Phys. Rev. B **82**, 085318 (2010).
[13] E. Bustarret, Physica C **514**, 36 (2015).
[14] L. Boeri, J. Kortus, and O. K. Andersen, Phys. Rev. Lett. **93**, 237002 (2004).
[15] Y. Ma, J. S. Tse, T. Cui, D. D. Klug, L. Zhang, Y. Xie, Y. Niu, and G. Zou, Phys. Rev. B **72**, 014306 (2005).
[16] K. Nakamura, S. H. Rhim, A. Sugiyama, K. Sano, T. Akiyama, T. Ito, M. Weinert, and A. J. Freeman, Phys. Rev. B **87**, 214506 (2013).
[17] A. Sugiyama, Master's thesis, Faculty of Engineering, Mie University, 2014.
[18] A. Sugiyama, K. Nakamura, K. Sano, T. Akiyama, and T. Ito, e-J. Surf. Sci. Nanotechnol. **12**, 109 (2014).
[19] B. G. Orr, H. M. Jaeger, and A. M. Goldman, Phys. Rev. B **32**, 7586 (1985).
[20] D. B. Haviland, Y. Liu, and A. M. Goldman, Phys. Rev. Lett. **62**, 2180 (1989).
[21] It might seem to be curious that the strength of E is above the electric breakdown threshold of diamond ($\sim 10^7$ V/cm). The same situation has been found in the experiment on the electric-field-induced superconductivity in $SrTiO_3$ [1]. However, there is a very strong electric field only near the surface, as shown in Fig. 1, and the electric field decays rapidly by the screening effect of the induced charge. Since most of the system remains as an insulator, a collision cascade of carriers that results in electric breakdown with a destructive effect to the whole system may not occur.
[22] P. G. Lurie and J. M. Wilson, Surf. Sci. **65**, 453 (1977).
[23] S. V. Pepper, J. Vac. Sci. Technol. **20**, 213 (1982).
[24] M. McGonigal, J. N. Russell, Jr., P. E. Pehrsson, H. G. Maguire, and J. E. Butler, J. Appl. Phys. **77**, 4049 (1995).
[25] P. Giannozzi, S. Baroni, N. Bonini, M. Calandra, R. Car, C. Cavazzoni, D. Ceresoli, G. L. Chiarotti, M. Cococcioni, I. Dabo, A. Dal Corso, S. Fabris, G. Fratesi, S. de Gironcoli, R. Gebauer, U. Gerstmann, C. Gougoussis, A. Kokalj, M. Lazzeri, L. Martin-Samos, N. Marzari, F. Mauri, R. Mazzarello, S. Paolini, A. Pasquarello, L. Paulatto, C. Sbraccia, S. Scandolo, G. Sclauzero, A. P. Seitsonen, A. Smogunov, P. Umari, and R. M. Wentzcovitch, J. Phys.: Condens. Matter **21**, 395502 (2009).
[26] The estimated effective mass is consistent with the result for boron-doped diamond ($m^* = 1.7$) obtained by V. A. Sidorov, E. A. Ekimov, S. M. Stishov, E. D. Bauer, and J. D. Thompson, Phys. Rev. B **71**, 060502(R) (2005).
[27] J. Bardeen, L. Cooper, and J. R. Schrieffer, Phys. Rev. **108**, 1175 (1957).
[28] A. Subedi and L. Boeri, Phys. Rev. B **84**, 020508(R) (2011).
[29] Using the 2D-like BZ as ($k \times k$), we can calculate λ of a 2D system, as well as of a 3D system, by using QE. See also Ref. [11] and J. Dai, Z. Li, J. Yang, and J. Hou, Nanoscale **4**, 3032 (2012).

[30] By using the rigid-muffin-tin approximation (RMTA) for C26H4, λ has been obtained as 0.18 and 0.47 at $|E| = 0.5$ and 1.0 V/Å, respectively [16]. Since the RMTA generally overestimates λ, the present results do not contradict the RMTA results. See also W. Ruesink, J. de Wilde, R. Griessen, and M. J. G. Lee, J. Phys. Colloq. **39**, C6-1097 (1978).

[31] W. L. McMillan, Phys. Rev. **167**, 331 (1968).

[32] P. B. Allen and R. C. Dynes, Phys. Rev. B **12**, 905 (1975).

[33] The size dependence of $\omega_{\log}$ is small and the obtained value is smaller than that of the bulk by $\sim$20%.

[34] S. Qin, J. Kim, Q. Niu, and C.-K. Shih, Science **324**, 1314 (2009); T. Uchihashi, P. Mishra, M. Aono, and T. Nakayama, Phys. Rev. Lett. **107**, 207001 (2011); A. D. Caviglia, S. Gariglio, N. Reyren, D. Jaccard, T. Schneider, M. Gabay, S. Thiel, G. Hammerl, J. Mannhart, and J.-M. Triscone, Nature (London) **456**, 624 (2008).

[35] T. Klein, P. Achatz, J. Kacmarcik, C. Marcenat, F. Gustafsson, J. Marcus, E. Bustarret, J. Pernot, F. Omnes, B. E. Sernelius, C. Persson, A. Ferreira da Silva, and C. Cytermann, Phys. Rev. B **75**, 165313 (2007).

[36] In our preliminary calculation without surface reconstruction, we find that the values of DOS of the (111)-surface and (100)-surface of diamond are smaller than that of the (110)-surface of diamond, and superconductivity may be not expected in these systems at $\sigma_c \sim 2.3 \times 10^{13}$ cm^{-2}.